CDF note 10120

Measurement of the Polarization Amplitudes of the $B_s^0 \to \phi\phi$ Decay

The CDF Collaboration
URL http://www-cdf.fnal.gov
(Dated: April 7, 2010)

We present the first measurement of the polarization amplitudes for the $B_s^0 \to \phi\phi$ decay. We use Tevatron data collected by the upgraded Collider Detector at Fermilab (CDF II) in the period starting from March 2001 till April 2008, which correspond to an integrated luminosity of 2.9 fb^{-1}. With a signal of approximately 300 $B_s^0 \to \phi\phi$ decays, we measure the three polarizations amplitudes and the cosine of the parallel amplitude strong phase:

$$|A_0|^2 = 0.348 \pm 0.041(\text{stat}) \pm 0.021(\text{syst}),$$
$$|A_\parallel|^2 = 0.287 \pm 0.043(\text{stat}) \pm 0.011(\text{syst}),$$
$$|A_\perp|^2 = 0.365 \pm 0.044(\text{stat}) \pm 0.027(\text{syst}),$$
$$\cos\delta_\parallel = -0.91^{+0.15}_{-0.13}(\text{stat}) \pm 0.09(\text{syst}).$$

The resulting polarization fractions are

$$f_\text{L} = 0.348 \pm 0.041(\text{stat}) \pm 0.021(\text{syst}),$$
$$f_\text{T} = 0.652 \pm 0.041(\text{stat}) \pm 0.021(\text{syst}).$$

I. INTRODUCTION

The $B_s^0 \to \phi\phi$ decay proceeds through a $b \to s\bar{s}s$ quark level process, and, in the Standard Model (SM), the dominant diagram is the $b \to s$ penguin (see FIG. 1). The same penguin amplitude is also relevant for several observables which have shown interesting deviation from the SM predictions like the difference in CP-violating asymmetries in $B^0 \to K^+\pi^-$ and $B^+ \to K^+\pi^0$ or the possible, albeit presently not significant, difference in the measurement of $\sin(2\beta)$ in $b \to s\bar{q}q$ and in $b \to c\bar{c}s$ B^0 decays. Similar comparison between $\sin(2\beta_s)$ measurements in $B_s^0 \to \phi\phi$ and $B_s^0 \to J/\psi\phi$ modes will be possible in the future. The first step in this direction is the measurement of the polarization in the $B_s^0 \to \phi\phi$ decay described here.

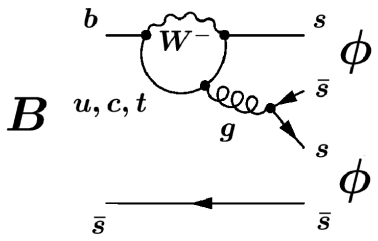

FIG. 1: $B_s^0 \to \phi\phi$ Feynman graph

The decay amplitude for this process, involving two vector mesons in the final state, can be expressed in terms of three independent amplitudes, which correspond to the three possible relative angular momenta L between the vector mesons [31]. The three *polarization* amplitudes (one longitudinal, $|A_0|^2$, and two transverse, $|A_\parallel|^2$ and $|A_\perp|^2$), can be measured from an analysis of the emission angles of the final states particles (*i. e.*, the decay products of the vector mesons). Since the final-state with a definite angular momentum is a CP-eigenstate, this decomposition allows investigation of the B_s^0 system CP-properties in the interference between decay and mixing and measurement of the B_s^0 decay width difference ($\Delta\Gamma_s$).

Taking into account the V-A nature of weak interaction and the helicity conservation in QCD, the SM predicts longitudinal polarization to be dominant with the transversely-polarized amplitudes suppressed by a factor m_V/m_B [1]. While this prediction is experimentally confirmed in the tree-level dominated $b \to u$ transition (such as $B^0 \to \rho^+\rho^-$ [2, 3], $B^+ \to \rho^0\rho^+$ [4], and $B^+ \to \omega\rho^+$ [5]) and there is evidence in $b \to d$ penguin transition ($B^0 \to \rho^0\rho^0$ [6]), in $B \to \phi K^\star$, a $\bar{b} \to \bar{s}$ penguin decay, it has been measured that the transverse polarization is about equal to the longitudinal one [7–9]. This surprising result is known as "Polarization Puzzle". It is then important to experimentally check what happens in other $\bar{b} \to \bar{s}$ penguin dominated decays like $B_s^0 \to \phi\phi$. Explanations involving either New Physics [10, 11] or corrections to naive expectation within the SM, due to penguin annihilation [1, 12, 13] or final state interactions [14–17], have been proposed. Moreover, within the penguin annihilation hypothesis it is possible to derive predictions for the $B_s^0 \to \phi\phi$ mode based on experimental information in SU(3) related B^0 modes and an estimate of SU(3) breaking [18].

In this report we present the first measurement of $B_s^0 \to \phi\phi$ polarization amplitudes using 300 $B_s^0 \to \phi\phi$ signal events reconstructed in 2.9 fb^{-1}of CDF II data. As a data-driven cross-check for our angular analysis we also measured polarizations of $B_s^0 \to J/\psi\phi$ decays collected by the same trigger that selects the $B_s^0 \to \phi\phi$ sample and compared the results with those known more precisely from an independent analysis [19].

Note that charge conjugate decay modes are implied throughout the rest of this document unless otherwise stated.

II. DECAY RATES

The following decay modes are considered: $B_s^0 \to \phi\phi \to [K^+K^-][K^+K^-]$ and $B_s^0 \to J/\psi\phi \to [\mu^+\mu^-][K^+K^-]$. We refer to the B_s^0 meson as the parent (or as the initial state) and to the two vector mesons as daughter particles (V_1 and V_2), and to their decay products as final state particles (P_1, P_2 from V_1, and P_3, P_4 from V_2) [32].

A. $B_s^0 \to \phi\phi$

In the $B_s^0 \to \phi\phi$ decay the two daughters are identical bosons. The natural angular basis respecting the Bose symmetry of the problem is the so-called helicity one: the x' (x'') axis is defined as the direction of the V_1 (V_2) momentum in the rest frame of the B_s^0; we define ϑ_1 (ϑ_2) as the angle between the x' (x'') axis and the P_1 (P_3) three-momentum vector, defined in the rest frame of their mother V_1 (V_2); the Φ angle is the angle between the decay planes of the two daughter particles. These angles, which form the vector $\vec{\omega} = (\cos\vartheta_1, \cos\vartheta_2, \Phi)$, are shown in FIG. 2.

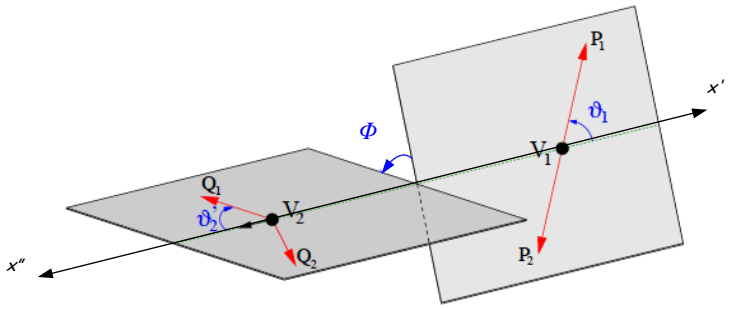

FIG. 2: Definitions of the helicity angles $\vec{\omega} = (\vartheta_1, \vartheta_2, \Phi)$ for a general $P \to V_1V_2$ decay. We identify $B_s^0 \to \phi\phi \to [K^+K^-][K^+K^-]$ with $P \to V_1V_2 \to [P_1P_2][Q_1Q_2]$.

The differential decay rate in terms of the helicity angles can be written as

$$\frac{d^4\Lambda(\vec{\omega}, t)}{dt d\vec{\omega}} = \frac{9}{32\pi} \sum_{i=1}^{6} K_i(t) f_i(\vec{\omega}), \tag{1}$$

where the angular functions $f_i(\vec{\omega})$ are given by

$$\begin{aligned}
f_1(\vec{\omega}) &= 4\cos^2\vartheta_1 \cos^2\vartheta_2, \\
f_2(\vec{\omega}) &= \sin^2\vartheta_1 \sin^2\vartheta_2 (1 + \cos 2\Phi), \\
f_3(\vec{\omega}) &= \sin^2\vartheta_1 \sin^2\vartheta_2 (1 - \cos 2\Phi), \\
f_4(\vec{\omega}) &= -2\sin^2\vartheta_1 \sin^2\vartheta_2 \sin 2\Phi, \\
f_5(\vec{\omega}) &= \sqrt{2}\sin 2\vartheta_1 \sin 2\vartheta_2 \cos\Phi, \\
f_6(\vec{\omega}) &= -\sqrt{2}\sin 2\vartheta_1 \sin 2\vartheta_2 \sin\Phi,
\end{aligned} \tag{2}$$

while the time-dependent functions $K_i(t)$ are defined as

$$
\begin{aligned}
K_1(t) =& \frac{1}{2}|A_0|^2\Bigg[(1+\cos\phi_{\rm s})e^{-\Gamma_{\rm L}t}+(1-\cos\phi_{\rm s})e^{-\Gamma_{\rm H}t}+2e^{-\Gamma t}\sin(\Delta m t)\sin\phi_{\rm s}\Bigg],\\
K_2(t) =& \frac{1}{2}|A_\parallel|^2\Bigg[(1+\cos\phi_{\rm s})e^{-\Gamma_{\rm L}t}+(1-\cos\phi_{\rm s})e^{-\Gamma_{\rm H}t}+2e^{-\Gamma t}\sin(\Delta m t)\sin\phi_{\rm s}\Bigg],\\
K_3(t) =& \frac{1}{2}|A_\perp|^2\Bigg[(1-\cos\phi_{\rm s})e^{-\Gamma_{\rm L}t}+(1+\cos\phi_{\rm s})e^{-\Gamma_{\rm H}t}-2e^{-\Gamma t}\sin(\Delta m t)\sin\phi_{\rm s}\Bigg],\\
K_4(t) =& |A_\parallel||A_\perp|\Bigg[e^{-\Gamma t}\Bigg(\sin(\delta_\perp-\delta_\parallel)\cos(\Delta m t)-\cos(\delta_\perp-\delta_\parallel)\sin(\Delta m t)\cos\phi_{\rm s}\Bigg)-\\
&-\frac{1}{2}\Bigg(e^{-\Gamma_{\rm H}t}-e^{-\Gamma_{\rm L}t}\Bigg)\cos(\delta_\perp-\delta_\parallel)\sin\phi_{\rm s}\Bigg],\\
K_5(t) =& \frac{1}{2}|A_0||A_\parallel|\cos(\delta_\parallel)\\
&\Bigg[(1+\cos\phi_{\rm s})e^{-\Gamma_{\rm L}t}+(1-\cos\phi_{\rm s})e^{-\Gamma_{\rm H}t}+2e^{-\Gamma t}\sin(\Delta m t)\sin\phi_{\rm s}\Bigg],\\
K_6(t) =& |A_0||A_\perp|\Bigg[e^{-\Gamma t}\Bigg(\sin\delta_\perp\cos(\Delta m t)-\cos\delta_\perp\sin(\Delta m t)\cos\phi_{\rm s}\Bigg)-\\
&-\frac{1}{2}\Bigg(e^{-\Gamma_{\rm H}t}-e^{-\Gamma_{\rm L}t}\Bigg)\cos\delta_\perp\sin\phi_{\rm s}\Bigg].
\end{aligned}
\tag{3}
$$

The time-dependent angular distribution for a $\bar{B}^0_s$ meson can be obtained by reversing the sign of the terms proportional to $\sin(\Delta m t)$ or $\cos(\Delta m t)$ in the $K_i(t)$ functions. The symbols are defined as follows:

- the three square moduli of the *polarization amplitudes* are $|A_0|^2$, $|A_\parallel|^2$ and $|A_\perp|^2$;
- the masses and widths of the two mass eigenstates are $M_{\rm H,L}$ and $\Gamma_{\rm H,L}$, and we define $\Delta m = M_{\rm H} - M_{\rm L}$, $\Gamma = 1/\tau_B = (\Gamma_{\rm L}+\Gamma_{\rm H})/2$ and $\Delta\Gamma = \Gamma_{\rm L} - \Gamma_{\rm H}$. For the B^0_s meson are taken as: $\tau_{\rm L} = 1/\Gamma_{\rm L} = 1.408^{+0.033}_{-0.030}$ ps, $\tau_{\rm H} = 1/\Gamma_{\rm H} = 1.543^{+0.058}_{-0.060}$ ps and $\Delta\Gamma_s = 0.062^{+0.034}_{-0.037}\,\text{ps}^{-1}$ [20].
- The phase $\phi_{\rm s}$ is the CP-violating weak phase $\phi_s^M - \phi(B^0_s \to \phi\phi)$ where ϕ_s^M is the B^0_s mixing amplitude phase and $\phi(B^0_s \to \phi\phi)$ is the phase of the amplitude ratio $\frac{A_{\bar{\phi}\phi}}{A_{\phi\phi}}$ of the $B^0_s \to \phi\phi$ decay; in the SM it is predicted to be extremely small since both terms are $2\arg(\rm V^*_{ts}V_{tb})$[21].
- The two strong phases: $\delta_\parallel = \arg(A_0^\star A_\parallel)$ and $\delta_\perp = \arg(A_0^\star A_\perp)$.

Assuming that

1. we do not attempt to distinguish a B^0_s meson from a $\bar{B}^0_s$ meson and thus we have to sum over the B^0_s and $\bar{B}^0_s$ terms of eq. 3. [33];
2. we have not the sensitivity to measure $\phi_{\rm s}$ and we assume its value in the SM [34], thus we fix $\phi_{\rm s} = 0$ in the $K_i(t)$ functions;

the differential angular decay rate of eq. 1 becomes

$$
\frac{d^4\Lambda(\vec{\omega},t)}{dt d\vec{\omega}} = \frac{9}{32\pi}\Bigg[\mathcal{F}_{\rm e}(\vec{\omega})\mathcal{K}_{\rm L}(t)+\mathcal{F}_{\rm o}(\vec{\omega})\mathcal{K}_{\rm H}(t)\Bigg],
\tag{4}
$$

where we distinguish two time-dependent and two angular-dependent terms:

$$
\mathcal{F}_{\rm e}(\vec{\omega}) = |A_0|^2 f_1(\vec{\omega}) + |A_\parallel|^2 f_2(\vec{\omega}) + |A_0||A_\parallel|\cos\delta_\parallel f_5(\vec{\omega}),
\tag{5a}
$$

$$
\mathcal{F}_{\rm o}(\vec{\omega}) = |A_\perp|^2 f_3(\vec{\omega}),
\tag{5b}
$$

$$
\mathcal{K}_{\rm L}(t) = 2e^{-\Gamma_{\rm L}t},
\tag{5c}
$$

$$
\mathcal{K}_{\rm H}(t) = 2e^{-\Gamma_{\rm H}t}.
\tag{5d}
$$

B. $B_s^0 \to J/\psi\phi$

The customary choice for the $B_s^0 \to J/\psi\phi$ angular analysis is the transversity basis. The three transversity angles form the vector $\vec{\Omega} = (\Theta, \Psi, \Phi)$, and they are defined as follows. In the rest frame of V_1, V_2 moves in the x direction; the z axis is perpendicular to the decay plane of $V_2 \to P_3P_4$ and we assume that the y-component of the P_3 three-momentum is non-negative. (Θ, Φ) are the angular coordinates of P_1 in the rest frame of V_1 and Ψ is that of P_2 in the rest frame of V_2 (see FIG. 3).

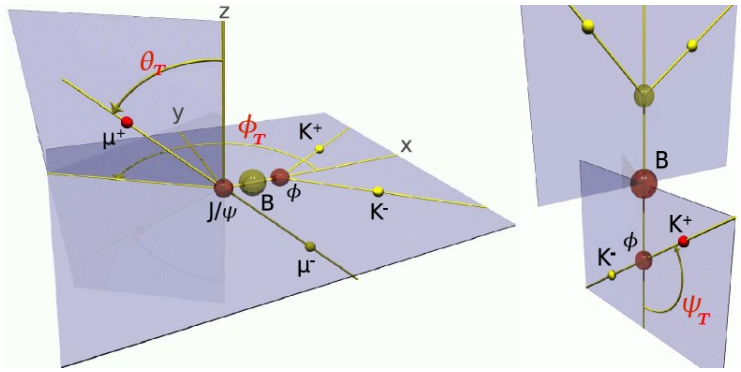

FIG. 3: Definitions of the transversity angles.

The differential angular decay rate has the same form of eq. 1, with the $f_i(\vec{\Omega})$ functions defined by

$$\begin{aligned}
f_1(\vec{\Omega}) &= 4\cos^2\Psi(1-\sin^2\Theta\cos^2\Phi),\\
f_2(\vec{\Omega}) &= \sin^2\Psi(1-\sin^2\Theta\sin^2\Phi),\\
f_3(\vec{\Omega}) &= \sin^2\Psi\sin^2\Theta,\\
f_4(\vec{\Omega}) &= -\sin^2\Psi\sin 2\Theta\sin\Phi,\\
f_5(\vec{\Omega}) &= \frac{1}{\sqrt{2}}\sin 2\Psi\sin^2\Theta\sin 2\Phi,\\
f_6(\vec{\Omega}) &= \frac{1}{\sqrt{2}}\sin 2\Psi\sin 2\Theta\cos\Phi,
\end{aligned} \tag{6}$$

and the $K_i(t)$ terms are obtained replacing ϕ_s with $\phi_s' = 2\beta_s = 2\arg(-V_{ts}V_{tb}^*/V_{cs}V_{cb}^*)$. As for $B_s^0 \to \phi\phi$, if we sum over B_s^0 and $\bar{B}_s^0$ terms and assume for β_s the SM value ($\beta_s \simeq 0$), we get for $B_s^0 \to J/\psi\phi$ analogous untagged decay rate as the one described by eq. 4.

III. DETECTOR TRIGGER AND DATA SAMPLE

The CDF II detector is described in detail elsewhere [22]. Most relevant to this analysis are the tracking and trigger systems. Three-dimensional charged particle tracking is achieved through an integrated system consisting of 6 layers of double-sided silicon detectors between 2.5 and 10 cm and 96 samplings in a large drift chamber (COT) [23] between 30 and 132 cm, all contained in a superconducting solenoid generating 1.41 T magnetic field. The muon detectors [24, 25] are used to collect the $B_s^0 \to J/\psi\phi$ decay sample; they have different transverse momentum thresholds due to geometry and material in front of them: for pseudo-rapidity $\eta \lesssim 0.6$, the CMU and CMP chambers are used, which can identify muons with $p_T > 1.5$ GeV/c, while, for pseudo-rapidity $0.6 \lesssim \eta \lesssim 1.0$, the CMX chambers have a threshold of approximately 2 GeV/c.

Hadronic B decays are collected via a dedicated track trigger capable of identifying tracks displaced from the primary vertex due to the long lifetime of b-hadrons. The online track reconstruction is performed at first level trigger in the COT by the XFT track processor [26] and by the Silicon Vertex Tracker (SVT) [27] at the second level. The latter combines the XFT and silicon detector informations achieving an impact parameter resolution comparable with the offline one.

The analysis described here uses a data sample selected requiring two charged tracks with transverse momenta $p_{\rm T} \geq 2$ GeV/c and with impact parameter 120 μm $\leq d_0 \leq$ 1000 μm. Furthermore the two trigger tracks must have an opening angle in the transverse plane satisfying $2^\circ \leq |\Delta\phi| \leq 90^\circ$ and $L_{xy} \geq 200$ μm, where the two dimensional decay length, L_{xy}, is calculated as the transverse distance from the beam line to the two track vertex projected along the total transverse momentum of the track pair. FIG. 4 shows a sketch of the relevant kinematic variables.

Three slightly different requirements on the scalar sum of track transverse momenta, $p_{\rm T1} + p_{\rm T2}$, define the three subsamples used for this measurement. That is `B_CHARM_LOWPT` requires $p_{\rm T1} + p_{\rm T2} > 4$ GeV/c, `B_CHARM_L1` ask for opposite charge tracks and $p_{\rm T1} + p_{\rm T2} > 5.5$ GeV/c while `B_CHARM_HIGHPT` ask for opposite charge tracks with $p_{\rm T1} + p_{\rm T2} > 6.5$ GeV/c. The three different subsamples are combined together after taking into account the different effective luminosity integrated by each trigger selection due to different trigger prescale factors.

In the text we will refer to *exclusive* trigger configurations. These are defined as follows:

- `HIGHPT`: only `B_CHARM_HIGHPT`;
- `ScA` (Scenario A) : events selected by `B_CHARM_L1` and not by `B_CHARM_HIGHPT`
- `LOWPT`: events selected by `B_CHARM_LOWPT` but not by `B_CHARM_L1` and by `B_CHARM_HIGHPT`.

Their percentages on the total sample are listed in TAB. I for both decays. We request the matching between at least two reconstructed tracks and the SVT tracks. The confirmation of the `B_CHARM_LOWPT` trigger selections is imposed.

Trigger Paths	Fractions	
	$B_s^0 \to \phi\phi$	$B_s^0 \to J/\psi\phi$
`HIGHPT`	0.39 ± 0.05	0.42 ± 0.02
`ScA`	0.38 ± 0.05	0.33 ± 0.02
`LOWPT`	0.22 ± 0.04	0.26 ± 0.02

TABLE I: Trigger paths fractions (exclusive selection).

The sample has been collected in the data taking period from the beginning of Run II till April 2008, and the integrated luminosity is 2.9 ± 0.2 fb^{-1}. We reconstruct the two body B_s^0 decay to two $\phi(1020)$ vector mesons with $\phi(1020) \to K^+K^-$ (BR=$49.2 \pm 0.6\%$ [20]), the final states thus consists of 4 charged kaons emerging from a single

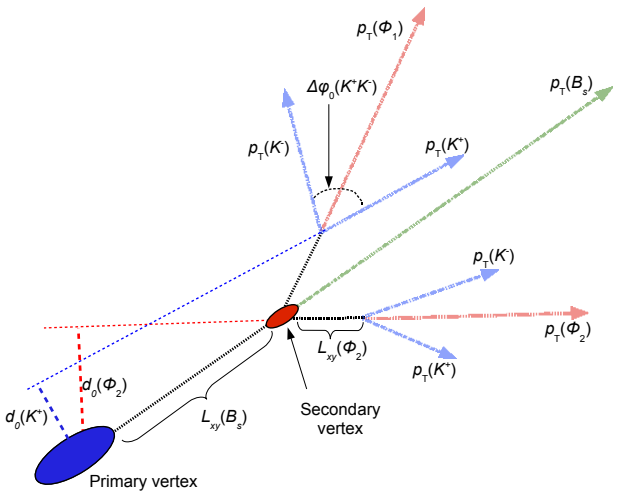

FIG. 4: Sketch of the $B_s^0 \to \phi\phi \to [K^+K^-][K^+K^-]$ decay projected into the transverse plane. Ellipses indicate vertexes, arrows indicate the transverse momenta (*i. e.*, the direction) of charged particles. Nothing is to scale.

displaced vertex. We reconstruct the $B_s^0 \to J/\psi\phi$ decay using the $J/\psi \to \mu^+\mu^-$ and $\phi(1020) \to K^+K^-$ decays which result in a $\mu^+\mu^-K^+K^-$ combination from a single displaced vertex. To reconstruct B_s^0 candidate all four-track combinations that satisfy trigger criteria are fit to a common vertex. All the tracks that are used in the vertex fit are required to have both drift chamber and silicon vertex hits and a minimum transverse momentum of 400 MeV/c.

Opposite charge track pairs with invariant mass within 15 MeV/c^2 from the $\phi(1020)$ mass PDG value [20] are considered $\phi(1020)$ candidates. In the case of the $B_s^0 \to J/\psi\phi$ vertex fit a mass constraint is also employed, requiring the invariant mass of the two muon candidates from J/ψ decay to be equal to the PDG J/ψ mass, 3097 MeV/c^2 [20]. This mass constraint significantly improves the invariant mass resolution of the measured $\mu^+\mu^-K^+K^-$ mass. At least one of the two tracks from the J/ψ decay is required to have a confirmation in the muon detectors, which are fully efficient for detecting muons with $p_{\rm T} > 1.5$ GeV/c. With this requirements an abundant and clean sample of $B_s^0 \to J/\psi\phi$ events is collected, keeping to a negligible level the contamination from $J/\psi \to e^+e^-$ decays.

IV. OPTIMIZATION PROCEDURE

Huge backgrounds due to random track combinations and to ϕ production from heavy flavor decays combined with two other random tracks need to be reduced in order to identify the $B_s^0 \to \phi\phi$ and the $B_s^0 \to J/\psi\phi$ signals. We inherit the set of cuts on discriminating variables form the branching ratio measurement[28]. We report here only the resulting selection requirements (TAB. II) on the following kinematic variables:

- for the $B_s^0 \to \phi\phi$ decay:
  - L_{xy}^B: transverse decay length of the reconstructed B;
  - d_0^B: impact parameter of the reconstructed B;
  - $d_0^{\phi_{\rm max}}$: impact parameter of the ϕ with higher momentum;
  - $p_{\rm T\,min}^K$: transverse momentum of the softer kaon;
  - χ^2_{xy}: χ^2 of the fit used in the reconstruction of the secondary vertex;
- for the $B_s^0 \to J/\psi\phi$ decay:
  - L_{xy}^B;
  - d_0^B;
  - $p_{\rm T}^\phi$: transverse momentum of the ϕ;
  - $p_{\rm T}^{J/\psi}$: transverse momentum of the J/ψ;
  - χ^2_{xy}.

Variables		Requirements	
		$B_s^0 \to \phi\phi$	$B_s^0 \to J/\psi\phi$
L_{xy}^B	[μm]	> 330	> 290
$p_{\rm T\,min}^K$	[GeV/c]	> 0.7	
$p_{\rm T}^\phi$	[GeV/c]		> 1.36
χ^2_{xy}		< 17	< 18
d_0^B	[μm]	< 65	< 65
$d_0^{\phi_{\rm max}}$	[μm]	> 85	
$p_{\rm T}^{J/\psi}$	[GeV/c]		> 2.0

TABLE II: Optimized selection cuts.

V. THE FINAL DATA SAMPLE

Applying the cuts listed in TAB. II, the invariant mass distributions, $m_{K^+K^-K^+K^-}$ for the $B_s^0 \to \phi\phi$ and $m_{K^+K^-\mu^+\mu^-}$ for the $B_s^0 \to J/\psi\phi$, are obtained (FIG. 5). These provide us with a first insight on the background and signal composition. In these distributions at least three components can be identified:

the signal: as expected, the signals appear as a narrow mass peak whose width is dominated by experimental resolution and whose yields are:

	$B_s^0 \to \phi\phi$	$B_s^0 \to J/\psi\phi$
Yield	295 ± 20	1766 ± 48

combinatorial background: these are random combinations of charged tracks accidentally satisfying the selection requirements. They produce a continuous invariant B_s^0 mass distribution and we expect a smooth slowing decreasing distribution in the signal region. It is the more important source of background in this analysis.

physics background: it is due to partially reconstructed heavy flavor decays or to an incorrect mass assignment to the tracks of other B meson decays (they are often referred to as *reflections*). We expect a distribution with a peak under the signal:

- for the $B_s^0 \to \phi\phi$: the decays that could produce reflections in the B_s^0 mass window are: $B^0 \to \phi K^\star \to [K^+K^-][K^+\pi^-]$ and $B_s^0 \to \bar{K}^\star K^\star \to [K^+\pi^-][K^+\pi^-]$; these reflections occur when the $K^\star$ is incorrectly reconstructed as a ϕ. The estimated number of reflection events is [28]:

	$B_s^0 \to \bar{K}^\star K^\star$	$B^0 \to \phi K^\star$
Events	0	8 ± 3
Fraction relative to the signal [%]	10^{-6}	3 ± 1

  Since its tiny percentage respect to the signal events, the $B^0 \to \bar{K}^\star K^\star$ reflection is neglected.
- for the $B_s^0 \to J/\psi\phi$: the dominant background decay is the $B^0 \to J/\psi K^\star \to [\mu^+\mu^-][K^+\pi^-]$ decay; it occurs when in the reconstruction the daughter tracks of the $K^\star$ are assumed to be two kaons and an incorrect invariant mass is computed. The estimated number of reflection events is [28]:

	$B^0 \to J/\psi K^\star$
Events	70 ± 20
Fraction relative to the signal [%]	4 ± 1

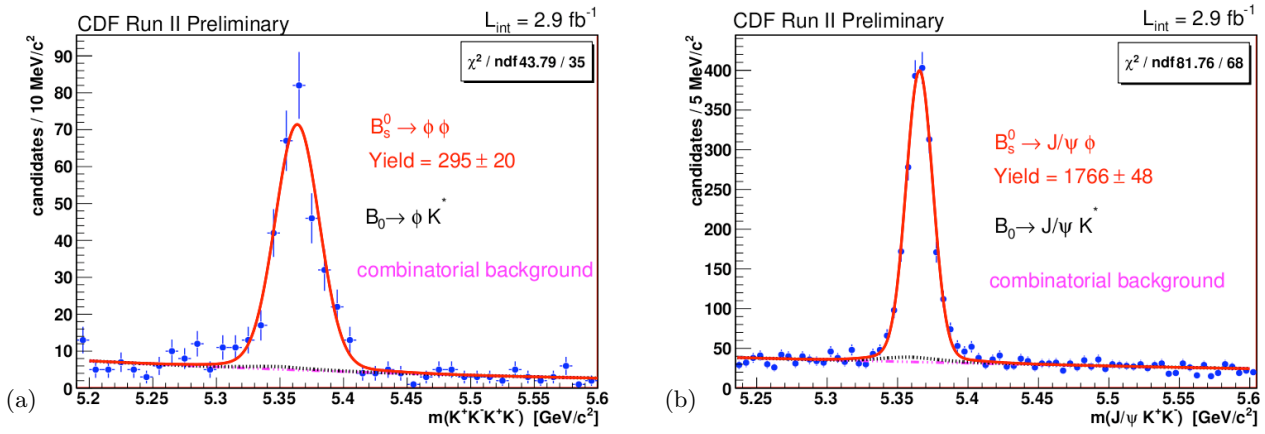

FIG. 5: Mass distributions of the $B_s^0 \to \phi\phi$ (a) and $B_s^0 \to J/\psi\phi$ (b) decays. The blue points represent data after the optimized selection; the red line is the total fit distribution; in black the reflection component; in purple the combinatorial background.

VI. FITTING TECHNIQUE

We measure the two polarization amplitudes, $|A_0|^2$ and $|A_\parallel|^2$ and the relative strong phase between them, $\delta_\parallel$, using as probability density function (pdf) the angular decay rate distribution of eq. 4 integrated in time. In eq. 4 we fix Γ_L

and Γ_H to the latest PDG values; moreover, the CP-violation's phase ϕ_s is set equal to zero and there is no distinction between B_s^0 and $\bar{B}_s^0$ at the production time (*untagged* analysis).

We perform an unbinned Maximum Likelihood (ML) fit using the following event observables::

- the reconstructed mass m of the B_s^0 candidate;
- the reconstructed angles
  - in the helicity basis, $\vec{\omega} = (\cos\vartheta_1, \cos\vartheta_2, \Phi)$, for the $B_s^0 \to \phi\phi$ decay;
  - in the transversity basis, $\vec{\Omega} = (\cos\Theta, \cos\Psi, \Phi)$, for the $B_s^0 \to J/\psi\phi$ decay;

The mass distribution is used in the fit to discriminate the signal from the background. The angles reconstruction starts from the momentum of the final state particles; in FIG. 6 the p_T distribution of the K^+ and K^- are shown.

In the $B_s^0 \to \phi\phi$ decay, the identification of the two ϕ as ϕ_1 and ϕ_2 (and then of the two angles ϑ_1 and ϑ_2) is randomly implemented in order to satisfy the symmetry of the variables under indexes exchange $1 \leftrightarrow 2$. Since the main purpose is the $B_s^0 \to \phi\phi$ angular analysis, in the following all the notations refer to its study, but the same procedure is adopted in the $B_s^0 \to J/\psi\phi$ study with obvious replacements.

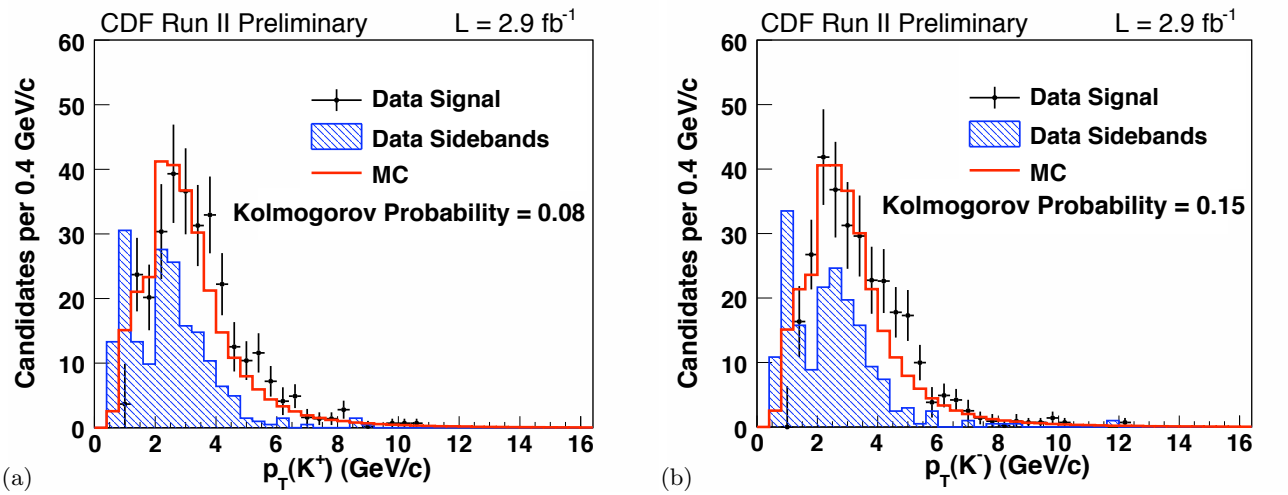

FIG. 6: p_T distribution for the K^+ (a) and K^- (b) particles for the $B_s^0 \to \phi\phi$. The black points are side-bands subtracted data; the red line is the MC; the blue histogram is the sidebands data distribution. The Kolmogorov probability for the comparison of Data and the MC distributions is 0.08 for (a) and it is 0.15 for (b).

The observables m and $\vec{\omega}$ define the vector of candidate observables $\vec{x}_i = (m_i, \vec{\omega}_i)$, where i spans over the number of events n. The Likelihood function is the product of the pdf g of the observables vector $\vec{x}$, for a given set of fit parameters $\vec{\xi}$,

$$\mathcal{L}(\vec{\xi}) = \prod_{i=1}^{n} g(\vec{x}_i; \vec{\xi}). \tag{7}$$

The pdf is the sum of two components: g_s, representing the signal set, and g_b, for the background events, *i. e.*,

$$g(\vec{x}_i; \vec{\xi}) = (1 - f_b) g_s(\vec{x}_i; \vec{\xi}_s) + f_b g_b(\vec{x}_i; \vec{\xi}_b), \tag{8}$$

where f_b is the fraction of background events ($0 \le f_b \le 1$). Since the mass and the angular variables are statistically independent, the pdf can be factorized in two corresponding terms, $g_{s(b)}^{(m)}$ and $g_{s(b)}^{(\omega)}$.

We evaluate the best parametrization of the pdf components and they are presented in the following sections. By using Monte Carlo (MC) simulation we are able to fix some parameters in the function parametrization and to make a global fit with a limited number of free parameters. We don't consider the reflection components in the background parametrization: since they are a tiny percentage of the total data sample, they can be neglected at first order. Thus, if it is not properly pointed out, when we refer to the background, we mean only the dominant combinatorial component.

A. Mass Model

The signal distribution has a width of around 20 MeV/c^2 for the $B_s^0 \to \phi\phi$ and of around 10 MeV/c^2 for the $B_s^0 \to J/\psi\phi$. In both cases, it is parametrized with two gaussian functions having the same mean value M but different resolutions, σ and $k\sigma$. This choice is fairly standard and takes into account the detector effects that cause an additional spread in the tail distributions. The function used to parametrize the distributions is the following:

$$g_{\rm s}^{(m)} = h\frac{1}{\sqrt{2\pi}\sigma}e^{-\frac{(m-M)^2}{2\sigma^2}} + (1-h)\frac{1}{\sqrt{2\pi}k\sigma}e^{-\frac{(m-M)^2}{2k^2\sigma^2}}, \tag{9}$$

where h is the fraction of one gaussian component with respect to the other. In the final fit the multiplicative factor k and the fraction h are fixed from the fit to large MC data sample, while the other parameters are left free.

The mass background follows, with a good approximation, an exponentially decreasing behavior:

$$g_{\rm b}^{(m)} = \frac{b}{e^{-bm_{\rm min}} - e^{-bm_{\rm max}}}e^{-bm}, \tag{10}$$

where b is the slope of the exponential function, and m spans the interval $[m_{\rm min} = 5.2, m_{\rm max} = 5.6]$ GeV/c^2.

B. Angular Model

The pdf used to describe the helicity angular distribution for the signal is obtained integrating in time the theoretical differential decay rate reported in eq. 4. The resulting signal angular pdf is

$$g_{\rm s}^{(\omega)} = \frac{d^3\Lambda(\vec{\omega})}{d\vec{\omega}} = \frac{9}{32\pi}\frac{1}{\tilde{W}}\left[\tilde{\mathcal{F}}_{\rm e}(\vec{\omega}) + \tilde{\mathcal{F}}_{\rm o}(\vec{\omega})\right], \tag{11}$$

where

$$\tilde{\mathcal{F}}_{\rm e} = \frac{2}{\Gamma_{\rm L}}\left[|A_0|^2 f_1(\vec{\omega}) + |A_\parallel|^2 f_2(\vec{\omega}) + |A_0||A_\parallel|\cos\delta_\parallel f_5(\vec{\omega})\right], \tag{12a}$$

$$\tilde{\mathcal{F}}_{\rm o} = \frac{2}{\Gamma_{\rm H}}|A_\perp|^2 f_3(\vec{\omega}), \tag{12b}$$

$$\tilde{W} = \frac{|A_0|^2 + |A_\parallel|^2}{\Gamma_{\rm L}} + \frac{|A_\perp|^2}{\Gamma_{\rm H}}. \tag{12c}$$

We expect to have a non uniform acceptance in the helicity (transversity) angles and we take this into account through an "angular acceptance" correction. The detector acceptance in the angular variables is estimated with the MC simulation. We use the phase space MC model, where the final state particles are generated averaging over all possible spin states. This results in the generation of uniform distributions in $\vec{\omega}$. The simulated events are passed through the full-fledged detector simulation. Then, they are selected with the same on-line and off-line requirements of the real data.

In practice, we construct the three-dimensional acceptance as a three-dimensional histogram $H(\vec{\omega})$, and the acceptance is calculated as the ratio between accepted and generated events in each three-dimensional bin in $\vec{\omega}$ divided by the total number of generated events such that the sum of the weights in all the bins of the histogram is 1. Thus, the acceptance function can be interpreted as the probability to find an event at each position in the $\vec{\omega}$ space. The projections of $H(\vec{\omega})$ in the three helicity (transversity) angles are shown in FIG. 7 for $B_s^0 \to \phi\phi$ (in FIG. 8 for $B_s^0 \to J/\psi\phi$). The robustness of this approach is validated in data by measuring $B_s^0 \to J/\psi\phi$ polarizations consistent with a set of published results (see the following section) in their turn cross-checked using $B^0 \to J/\psi K^{0\star}$ decay.

The angular acceptance effect is finally taken into account by the multiplicative term $\mathcal{H}(\vec{\omega})$ in the signal angular pdf:

$$g_{\rm s}^{(\omega)} = \frac{d^3\Lambda(\vec{\omega})}{d\vec{\omega}} \to g_{\rm s}^{(\omega)} = \frac{1}{\mathcal{N}}\frac{d^3\Lambda(\vec{\omega})}{d\vec{\omega}}\mathcal{H}(\vec{\omega}) \tag{13}$$

where $\mathcal{N}$ is a normalization term.

Finally, we use a purely empirical parametrization derived by analysing the angular distributions in the mass sidebands to model the background [35]. Assuming that the background pdf factorizes for the three angles, the pdf is a constant in the ϕ angle and is parameterized as $1 + B\cos^2\vartheta$ for the ϑ_1 and ϑ_2.

Finally, before carrying out the fit over the data sample of $B_s^0 \to \phi\phi$, the fitter was extensively tested and validated using simulated samples.

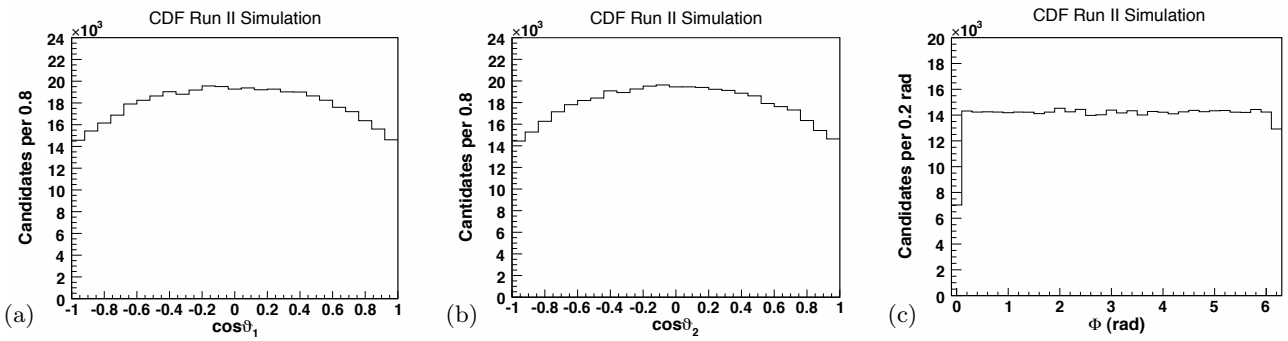

FIG. 7: Detector angular acceptance projections for $B_s^0 \to \phi\phi$: $\cos\vartheta_1$ (a), $\cos\vartheta_2$ (b) and Φ (c).

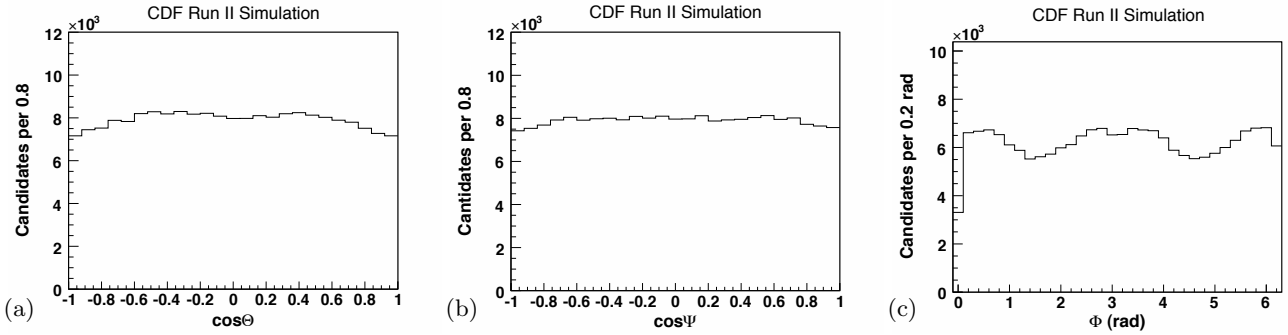

FIG. 8: Detector angular acceptance projections for $B_s^0 \to J/\psi\phi$: $\cos\Theta$ (a), $\cos\Psi$ (b) and Φ (c).

VII. FIT TO $B_s^0 \to J/\psi\phi$ SAMPLE FROM THE DISPLACED TRACK TRIGGER

We use the $B_s^0 \to J/\psi\phi$ decay mode as a control sample, which serves the purpose of improving the reliability of the main analysis. The results of the fit performed on 2.9 fb^{-1}of data for the $B_s^0 \to J/\psi\phi$ are listed in the TAB. III, and the fit projections onto the three transversity angles are shown in fig. 9. We compare the results with the ones obtained in the analysis published in [19], whose data were collected by the CDF II detector between February 2002 and January 2007 with the Dimuon trigger selection, and correspond to an integrated luminosity of 1.7 fb^{-1}. The fit results are in agreement with the published ones, thus confirming the reliability of our angular analysis.

Parameter	Displaced Track sample	Dimuon sample
$\lvert A_0\rvert^2$	0.534 ± 0.019(stat)	0.531 ± 0.020(stat) ± 0.007(syst)
$\lvert A_\parallel\rvert^2$	0.220 ± 0.025(stat)	0.239 ± 0.029(stat) ± 0.011(syst)

TABLE III: Comparison of our fit results and the ones in [19] for $B_s^0 \to J/\psi\phi$.

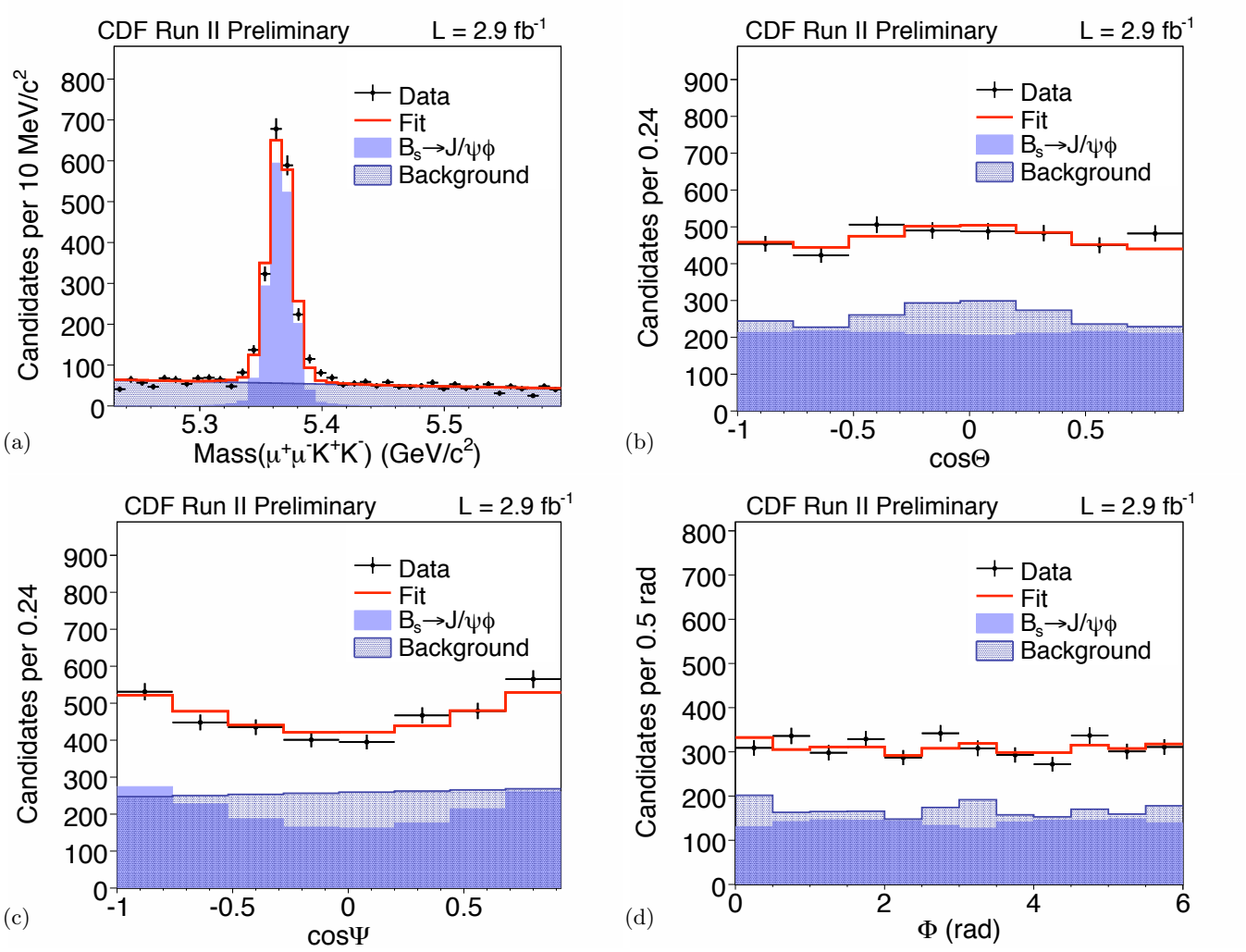

FIG. 9: Angular fit projections for $B_s^0 \to J/\psi\phi$: mass (a), $\cos\Theta$ (b), $\cos\Psi$ (c) and Φ (d).

VIII. FIT RESULTS

The results of the fit performed on 2.9 fb^{-1}of data for the $B_s^0 \to \phi\phi$ are finally listed in the TAB. IV and the correlation coefficients are listed in TAB. V. Note that the fit estimates for $\cos\delta_{\|}$ is in the physical region. The fit projections onto the three helicity angles are shown in FIG. 10: we see that the data distributions are very well reproduced by the fitting functions. The contour-plots for the three polarization parameters are shown in fig. 11. These contour-plots provide the actual coordinates of the points around the contour calculated at the level $-2\log(\mathcal{L}(\vec{\xi}_{\rm min}))+2.3$ which corresponds to the Confidence Level of 68.3%.

Parameter	Fit value
M [GeV/c^2]	5.3636 ± 0.0012
σ [GeV/c^2]	0.0165 ± 0.0011
$f_{\rm b}$	0.381 ± 0.030
b [c^2/GeV]	2.68 ± 0.67
$\lvert A_0\rvert^2$	0.348 ± 0.041
$\lvert A_{\|}\rvert^2$	0.287 ± 0.043
$\cos\delta_{\|}$	$-0.91^{+0.15}_{-0.13}$
B	$0.49^{+0.31}_{-0.26}$

TABLE IV: Results of the $B_s^0 \to \phi\phi$ fit.

	M	σ	$f_{\rm b}$	b	$\lvert A_0\rvert^2$	$\lvert A_\parallel\rvert^2$	$\cos\delta_\parallel$	B
M	+1.000	−0.047	+0.049	+0.070	+0.002	−0.008	−0.010	+0.010
σ	−0.047	+1.000	−0.357	−0.022	+0.055	−0.025	+0.110	+0.036
$f_{\rm b}$	+0.029	−0.357	+1.000	+0.020	−0.064	+0.023	−0.147	−0.034
b	+0.070	−0.022	+0.020	+1.000	−0.005	−0.002	−0.000	+0.003
$\lvert A_0\rvert^2$	+0.002	+0.055	−0.064	−0.005	+1.000	−0.447	+0.133	−0.217
$\lvert A_\parallel\rvert^2$	−0.008	−0.025	+0.023	−0.002	−0.447	+1.000	+0.092	+0.106
$\cos\delta_\parallel$	−0.010	+0.110	−0.147	−0.000	+0.133	+0.092	+1.000	+0.025
B	+0.010	+0.036	−0.034	+0.003	−0.217	+0.106	−0.025	+1.000

TABLE V: Correlation coefficients of the $B_s^0 \to \phi\phi$ fit.

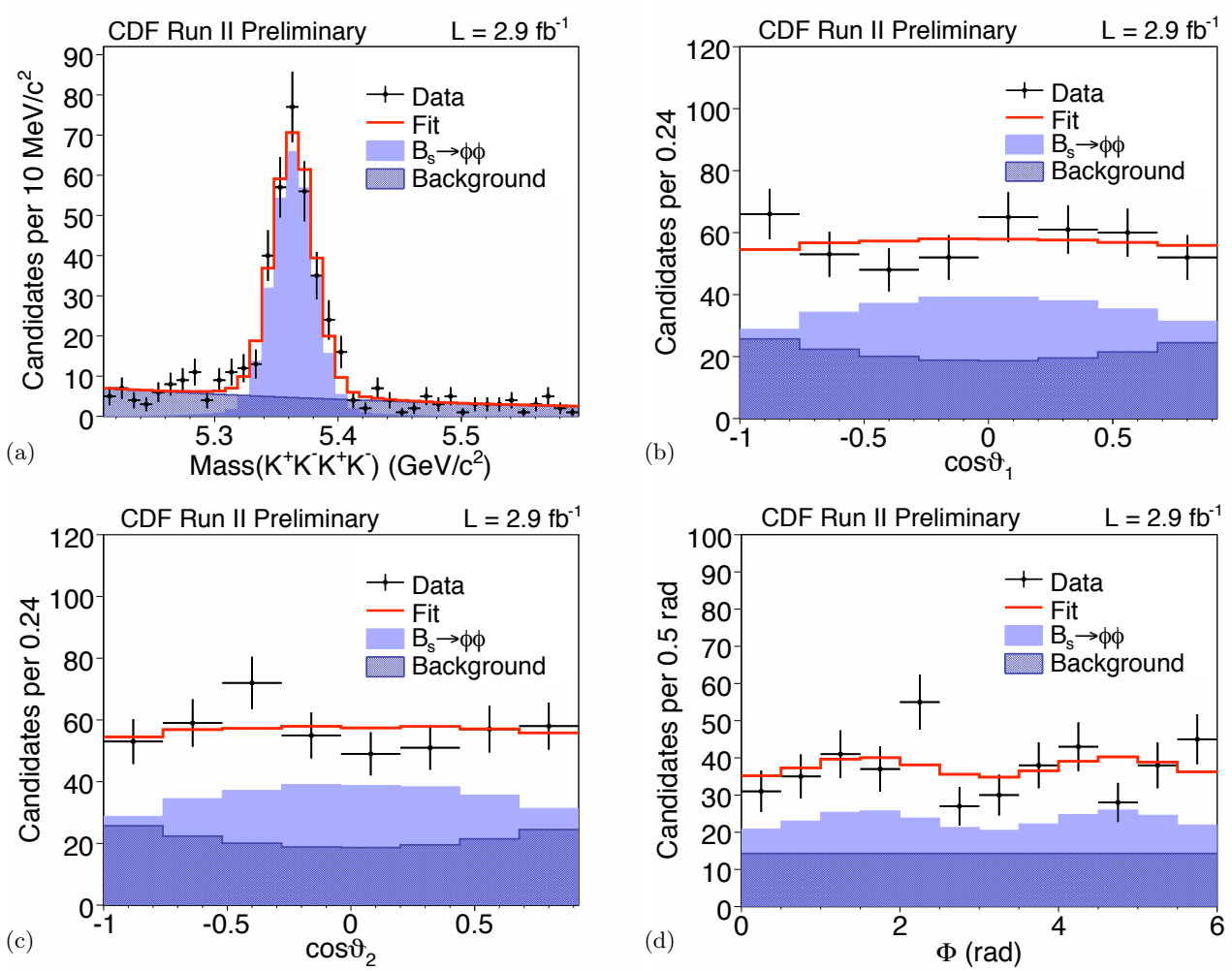

FIG. 10: Projections of the fit for $B_s^0 \to \phi\phi$: mass (a), $\cos\vartheta_1$ (b), $\cos\vartheta_2$ (c) and Φ (d).

IX. SYSTEMATIC UNCERTAINTIES

We consider the following systematic sources.

Residual discrepancy Data-MC. In the MC validation performed in the branching ratio analysis [28], we saw a small discrepancy between the data and MC $p_{\rm T}(B)$ distribution. Then, we find a reweighing function (see [28]) and we reweigh the 3D histogram of angular signal acceptance in the final fit. We evaluate how this changes the fit estimates.

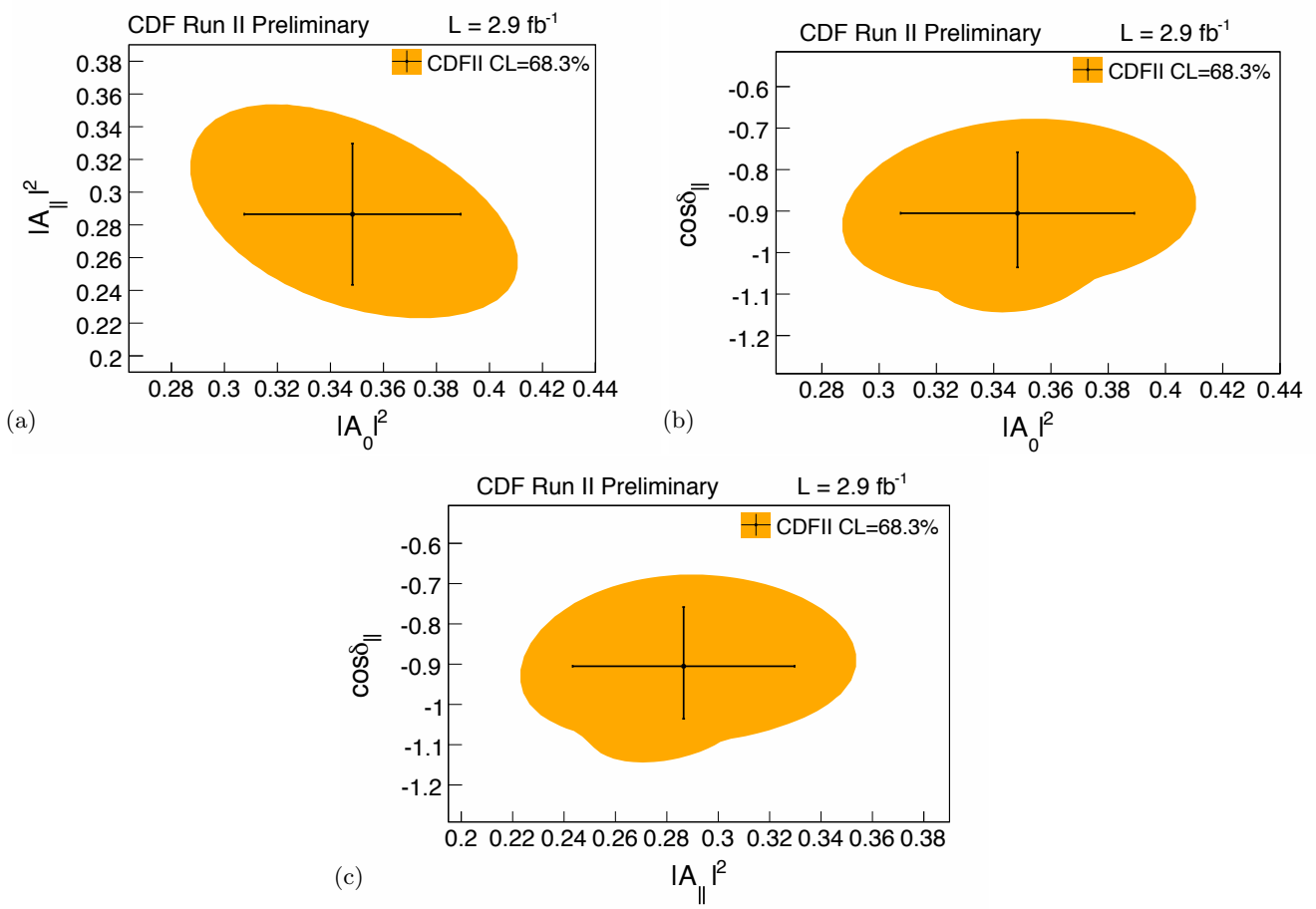

FIG. 11: Contour-plots of the fit for $B_s^0 \to \phi\phi$: $|A_0|^2$ versus $|A_\parallel|^2$ (a), $|A_0|^2$ versus $\cos\delta_\parallel$ (b) and $|A_\parallel|^2$ versus $\cos\delta_\parallel$ (c). The crosses are the fit estimates with statistical errors.

Binning of angular acceptance histogram. Since the signal angular acceptance is taken from a 3D histogram, we account for any dependence of the fit estimates on its binning.

Angular acceptance model (Trigger-Paths division). Since we fill the angular acceptance histogram with the events coming from the sum of the three exclusive trigger-paths data set, we consider the potential bias introduced by the trigger differences in the angular acceptance model.

Angular background model. We study the impact of the specific angular background model used with respect to different parameterizations.

Reflection background component. In the fit we do not include the $B^0 \to \phi K^\star$ reflection component. Anyway, we have evaluated its fraction in our data sample as in [28]. We can then estimate the effect of this background by using a Monte Carlo simulation with the measured value for polarizations of the $B^0 \to \phi K^\star$ decay.

***ct*-dependence of angular acceptance.** We estimate the impact on the fit estimates of some detector angular acceptance dependencies on ct.

Satellite Peak. We evaluate the effect of potential reflections or other peaking background that might be hiding on the low mass side of the signal peak.

Non-resonant contribution. We account for possible small S-wave (scalar) contribution to the angular distribution, due to non-resonant components under the ϕ peak signal, or a resonant contribution such as a $f_0\phi$ final state. We decided to generate MC for two possible (main) S-wave contribution that might leak under our signal:

1. B_s^0 to ϕ and a non resonant pair of Kaons ($B_s^0 \to \phi(K^+K^-)$);
2. B_s^0 to ϕ and an f_0 which in turn decays into the K^+K^- channel ($B_s^0 \to \phi f_0$).

We normalize the fraction of such contributions with respect to the signal yield considering the analogy with the B^0 case; we estimate the effect of the possible contribution of these backgrounds by assuming a 0.9 % contamination for the $B_s^0 \to \phi(K^+K^-)$ and 4.6% for the $B_s^0 \to \phi f_0$ one.

Dependence of the Angular Acceptance on $\Delta\Gamma_s$. If the width difference $\Delta\Gamma_s$ is sizable (as expected and verified experimentally) a significant bias on the polarization at $t = 0$ (the physical observable) is expected when performing a time integrated measurement. Assuming world average value for $\Gamma_{\rm H}$ and $\Gamma_{\rm L}$, we evaluate the effect coming purely from the normalization of the decay rate; we need to additionally consider the effect induced by a non uniform acceptance with the B_s^0 decay proper time introduced by the two displaced track trigger as well. The Monte Carlo simulation reproduces the ct acceptance of the trigger and selection reasonably well for the purpose we are interested here. The assigned systematic is the full shift, due to the non uniform ct acceptance, expected in the measured polarization assuming a value for $\Delta\Gamma_s$ equal to the the world average + 1σ [20].

$\tau_{\rm L}$ and $\tau_{\rm H}$ uncertainties We consider the propagation of the $\tau_{\rm L(H)}$ uncertainties to the polarization amplitudes.

CP-violation dependence. In our fit we assume to be in the SM, thus, we fix the CP-violation $\phi_{\rm s} = 0$. We evaluate how this assumption affects the fit estimates.

We summarize the systematic uncertainties in the following table

	$\lvert A_0\rvert^2$ syst	$\lvert A_\parallel\rvert^2$ syst	$\lvert A_\perp\rvert^2$ syst	$\cos\delta_\parallel$ syst
MC reweight	±0.003	±0.001	±0.002	±0.007
Acceptance binning	±0.001	±0.001	±0.000	±0.004
Acceptance Model	±0.005	±0.002	±0.003	±0.005
Background Model	±0.001	±0.001	±0.002	±0.009
Acceptance ct-dependence	±0.000	±0.001	±0.001	±0.004
Reflection component	±0.008	±0.002	±0.006	±0.019
Non-resonant contribution	±0.013	±0.003	±0.010	±0.084
Satellite peak	±0.004	±0.000	±0.004	±0.020
Acceptance $\Delta\Gamma$-dependence	±0.009	±0.009	±0.016	±0.011
$\tau_{\rm L(H)}$ uncertainties	±0.008	±0.006	±0.017	
CP-violation	±0.002	±0.001	±0.003	±0.009
total	±0.021	±0.011	±0.027	±0.090

X. FINAL RESULTS AND CONCLUSIONS

We have presented the first measurement of the polarization amplitudes for the charmless $B_s^0 \to \phi\phi$ decay of the B_s^0 meson. The results for the polarization amplitudes and the cosine of the strong parallel phase are

$$\begin{aligned}
|A_0|^2 &= 0.348 \pm 0.041(\text{stat}) \pm 0.021(\text{syst}),\\
|A_\parallel|^2 &= 0.287 \pm 0.043(\text{stat}) \pm 0.011(\text{syst}),\\
|A_\perp|^2 &= 0.365 \pm 0.044(\text{stat}) \pm 0.027(\text{syst}),\\
\cos\delta_\parallel &= -0.91^{+0.15}_{-0.13}(\text{stat}) \pm 0.09(\text{syst}).
\end{aligned}$$

The resulting polarization fractions are

$$\begin{aligned}
f_{\rm L} &= 0.348 \pm 0.041(\text{stat}) \pm 0.021(\text{syst}),\\
f_{\rm T} &= 0.652 \pm 0.041(\text{stat}) \pm 0.021(\text{syst}).
\end{aligned}$$

In conclusion, we find that also in the $b \to s$ penguin decay $B_s^0 \to \phi\phi$ the longitudinal fraction is not dominant like in previously studied B^0 and $B^\pm$ decays and contrary to naive expectation. We compare in TAB. VI the measured fraction with recent theoretical calculations.

Acknowledgments

We thank the Fermilab staff and the technical staffs of the participating institutions for their vital contributions. This work was supported by the U.S. Department of Energy and National Science Foundation; the Italian Istituto

	$f_{\rm L}$ [%]
CDF Run II	$34.8 \pm 4.1(\text{stat}) \pm 2.1(\text{syst})$
QCD factorization 1	48^{+0+26}_{-0-27}
QCD factorization 2	34 ± 28
QCD factorization 3	86.6
Naive factorization	88.3
NLO EWP 1	86.3
NLO EWP 2	86.3
perturbative QCD	$61.9^{+3.6+2.5+0.0}_{-3.2-3.3-0.0}$

TABLE VI: $B_s^0 \to \phi\phi$ longitudinal polarization fraction $f_{\rm L}$: comparison with theoretical predictions. The references are: [1] for QCD factorization 1, [18] for QCD factorization 2, [29] for QCD factorization 3 and Naive factorization, [30] for NLO EWP 1 and 2, [12] for perturbative QCD.

Nazionale di Fisica Nucleare; the Ministry of Education, Culture, Sports, Science and Technology of Japan; the Natural Sciences and Engineering Research Council of Canada; the National Science Council of the Republic of China; the Swiss National Science Foundation; the A.P. Sloan Foundation; the Bundesministerium für Bildung und Forschung, Germany; the World Class University Program, the National Research Foundation of Korea; the Science and Technology Facilities Council and the Royal Society, UK; the Institut National de Physique Nucleaire et Physique des Particules/CNRS; the Russian Foundation for Basic Research; the Ministerio de Ciencia e Innovación, and Programa Consolider-Ingenio 2010, Spain; the Slovak R&D Agency; and the Academy of Finland.

[1] Martin Beneke and Johannes Rohrer and Deshan Yang. Branching fractions, polarisation and asymmetries of $B \to VV$ decays. *Nuclear Physics B*, 774(1-3):64 – 101, 2007.
[2] Belle Collaboration. *Phys. Rev. Lett.*, 96:171801, 2006.
[3] BABAR Collaboration. A Study of $B^0 \to \rho^+\rho^-$ Decays and Constraints on the CKM Angle α. *Physical Review D*, 76:052007, 2007.
[4] BABAR Collaboration. Measurements of Branching Fraction, Polarization, and Charge Asymmetry of $B^\pm \to \rho^\pm\rho^0$ and a Search for $B^\pm \to \rho^\pm f^0(980)$. *Physical Review Letters*, 97(26):261801, 2006.
[5] BABAR Collaboration. B meson decays to $\omega K^\star$, $\omega\rho$, $\omega\omega$, $\omega\phi$, and ωf^0. *Physical Review D (Particles and Fields)*, 74(5):051102, 2006.
[6] BABAR Collaboration. Evidence for $B^0 \to \rho^0\rho^0$ Decays and Implications for the Cabibbo-Kobayashi-Maskawa Angle α. *Physical Review Letters*, 98(11):111801, 2007.
[7] The BABAR Collaboration. Vector-Tensor and Vector-Vector Decay Amplitude Analysis of $B^0 \to \phi K^\star$. *Physical Review Letters*, 98:051801, 2007.
[8] The BABAR Collaboration. Measurements of Branching Fractions, Polarizations, and Direct CP-Violation Asymmetries in $B \to \rho K^\star$ and $B \to f^0(980)K^\star$ Decays. *Physical Review Letters*, 97(20):201801, 2006.
[9] K. F. Chen for the Belle Collaboration. Measurement of Polarization and Triple-Product Correlations in $B \to \phi K^\star$ Decays. *Physical Review Letters*, 94:221804, 2005.
[10] Ezequiel Alvarez, Luis N. Epele, Daniel Gomez Dumm, and Alejandro Szynkman. Right handed currents and FSI phases in $B^0 \to \phi K^{\star 0}$. *Physical Review D*, 70:115014, 2004.
[11] C. S. Kim and Ya-Dong Yang. Polarization Anomaly in $B \to \phi K^{\star 0}$ and Probe of Tensor Interactions, 2004.
[12] Ahmed Ali, Gustav Kramer, Ying Li, Cai-Dian Lu, Yue long Shen, Wei Wang, and Yu-Ming Wang. Charmless non-leptonic B_s decays to PP, PV and VV final states in the pQCD approach. *Physical Review D*, 76:074018, 2007.
[13] Alexander L. Kagan. Polarization in $B \to VV$ decays. *Phys. Lett. B*, 601:151–163, 2004.
[14] P. Colangelo, F. De Fazio, and T. N. Pham. The riddle of polarization in $B \to VV$ transitions. *Phys. Lett. B*, 597:291–298, 2004.
[15] Massimo Ladisa, Vincenzo Laporta, Giuseppe Nardulli, and Pietro Santorelli. Final state interactions for $B \to VV$ charmless decays. *Phys. Rev.D*, 70:114025, 2004.
[16] Hai-Yang Cheng, Chun-Khiang Chua, and Amarjit Soni. Final state interactions in hadronic B decays. *Phys. Rev.D*, 71:014030, 2005.
[17] Christian W. Bauer, Dan Pirjol, Ira Z. Rothstein, and Iain W. Stewart. $B \to M(1)M(2)$: Factorization, charming penguins, strong phases, and polarization. *Phys. Rev. D*, 70:054015, 2004.
[18] Alakabha Datta, David London, Joaquim Matias, Makiko Nagashima, and Alejandro Szynkman. Final-state Polarization in Bs Decays. *Eur. Phys. J. C*, 60:279–284, 2009.
[19] CDF Collaboration. Measurement of Lifetime and Decay-Width Difference in $B_s^0 \to J/\psi\phi$ Decays. *Physical Review Letters*, 100:121803, 2008.
[20] C. Amsler et al. Particle Data Group. *Physics Letters B*, 667, 2008 and 2009 partial update for the 2010 edition.

[21] Martti Raidal. CP asymmetry in B –¿ Phi K(S) decays in left-right models and its implications on B/s decays. *Phys. Rev. Lett.*, 89:231803, 2002.
[22] R. Blair and others (CDF II Collaboration). The CDF II Detector, Technical Design Report. *FERMILAB-Pub-96/390-E CDF*, 1996.
[23] A. Affolder et al. CDF Central Outer Tracker. *Nucl. Instrum. Methods*, A526, 2004.
[24] G. Ascoli et al. CDF central muon detector. *Nucl. Instrum. Methods*, A268, 1988.
[25] C. M. Ginsburg et al. CDF Run 2 Muon System. *Eur. Phys. J.*, 33(S1002), 2004.
[26] E. J. Thomson et al. Online Track Processor for the CDF Upgrade. *IEEE Trans. Nucl. Sci.*, 49, 2002.
[27] B. Ashmanskas et al. The CDF Silicon Vertex Trigger. *Nucl. Instrum. Methods*, A518, 2004.
[28] The CDF collaboration. Updated Measurement of the $B_s \to \phi\phi$ Branching Ratio Using 2.9 fb^{-1}. *CDF Public Note*, 10064, 2010. unpublished.
[29] Xinqiang Li, Gongru Lu, and Yadong Yang. Charmless $\bar{B}_s \to VV$ Decays in QCD Factorization. *ERRATUM-IBID.D*, 71:019902, 2005.
[30] D. Du and L. Guo. *J. Phys. G: Nucl. Part. Phys.*, 23:525, 1997.
[31] In fact, for two spin 1 particles, L can be equal to 0, 1, or 2 to obtain the spin 0 initial state.
[32] Fix the following convention: if the final states are charged particles, P_1 and P_3 are the positive charged ones.
[33] We are supposing that B_s^0 and $\bar{B}_s^0$ are produced in equal numbers at the Tevatron.
[34] We evaluate the impact of this assumption in the systematics treatment.
[35] Considering the B_s^0 mass distribution, the sidebands are the region from 5.02 to 5.22 GeV/c^2 and from 5.52 to 5.72 GeV/c^2.